Electronic Supplementary Material (ESI) for Sensors & Diagnostics.

Supporting Information

Self-assembled Emissive Probe for Efficient Sensing of Fe(III) and Cysteine in the Physiological Medium: Application in Real Water and Food Sample

Sulekha Kumari Pandit, Sanjana Das and Gopal Das*

Department of Chemistry, Indian Institute of Technology Guwahati, Assam, 781039, India

E-mail: gdas@iitg.ac.in

General Information and Materials

The UV-Visible absorption spectra were recorded using quartz cuvettes with a 10-mm path length and wavelengths ranging from 250 nm to 600 nm on a Perkin-Elmer Lamda-750 UV-Vis spectrophotometer. For all spectra, baseline correction was utilized.

On a Horiba Fluoromax-4 spectrofluorometer, fluorescence emission spectra were recorded using quartz cuvettes with a 1 cm path length and a 5 nm slit width operating at 298 K. Samples were excited at 350 nm and emission was taken in the range from 365-600 nm.

Agilent LC_QTOF_HRMS Premier mass spectrometer was used to perform high-resolution mass spectrometry on PAM and PAD. Using a Bruker Advances 600 NMR apparatus was used as the solution-phase ^{1}H and ^{13}C Nuclear Magnetic Resonance (NMR) spectra. With the deuterated solvents, the chemical shifts were recorded in parts per million (ppm). In ^{1}H NMR spectra, spin multiplicities are indicated by the following abbreviations: s = singlet, d = doublet, t = triplet and q = quartet, coupling constant (s) in Hz

(FTIR) measurements of the samples were recorded with Bruker VERTEX 70v FTIR spectrometer.

The various salts, solvents, starting materials, and reagents were all purchased from commercial suppliers and used exactly as they were given. They were all of the reagent grade. HPLC grade solvents were employed. Deuterated solvent [$(CD_3)_2SO$] was bought from Sigma-Aldrich for NMR investigations. The metal ions including salts $AgCl_2$, $Zn(OAc)_2$, $Cu(OAc)_2$, $HgCl_2$, $CrCl_3$, $Cd(OAc)_2$, $Pb(OAc)_2.3H_2O$, $Mn(OAc)_2$, $Co(OAc)_2$, $AlCl_3$ and $FeCl_3$ from Sigma-Aldrich.

Synthesis of 2- (4-aminophenyl) - 1H-benzo [de] isoquinoline-1,3 (2H) - dione (Nap-1)

Nap-1 was synthesized via the reported procedure [1]**.** 1,8-naphthalic anhydride (0.5 g, 2.52 mmol) was added to a mixture of p- phenylenediamine (0.545 g, 5.04 mmol) in C_2H_5OH (100 mL), and the reaction mixture was reflux for 48 h. After reaction was completed, the solvent was filtered. The crude product was elution with ethanol afforded Nap-1 as a Greenish-brown solid (72% yield).

Fluorescence spectral studies for Fe (III) detection

The probe PAM and PAD stock solutions were made in DMSO at a concentration of 5×10^{-3} M and diluted to 5 μM. Metal salts of different cations (0.05 M) were produced in DMSO, for aqueous medium selectivity investigations and diluted suitably for subsequent experiments. In fluorescence studies, a quartz optical cell with a pathlength of 10 mm was filled with a 2.0 mL

solution of probe and various cations of stock solutions were gradually added with the aid of a micropipette. Excitation was given at 350 nm for PAM and PAD, respectively. For standard selectivity and titration experiments, emission was measured from 365 to 600 nm. Within 1 minutes of adding the external ions, spectral data were collected. All experiments were conducted in aqueous HEPES Buffer.

Stern-Volmer Plot

The Stern-Volmer equation was used to investigate the turn-on behaviour.

$I_o/I=1+K_{sv}$ [G] (1)

where I_o, I are the fluorescence intensities before and after addition of the anion, K_{sv} is the Stern- Volmer rate constant and [G] is the concentration of the guest.

Limit of Detection (LOD)

The detection limit for guest was determined using fluorescence titration changes. The fluorescence emission spectra of Nap-1 was computed 5 times, and the standard deviation of the blank measurement was calculated. To determine the slope, the fluorescence emission at 398 nm was plotted as a function of guest concentration. The following equation was used to compute the detection limits:

$LOD = 3\sigma/K$ (2)

where σ is the standard deviation of blank measurement, and k is the slope between the fluorescence emission intensity versus [Guest].

Quantum Yield Calculation

The quantum yield (Φ) was measured by comparing the integrated photoluminescence intensities and the absorbency values with the reference quinine sulfate (QS). The quinine sulfate (literature Φ = 0.54) was dissolved in 0.1 M H_2SO_4 (refractive index (η) of 1.33) and the receptors were dissolved in distilled water (η = 1.33). Where Φ is the quantum yield, I is the measured integrated emission intensity, η is the refractive index. A_R and A represents the absorbance at the excitation wavelength of 340 nm of the quinine sulfate and receptors respectively. The subscript R refers to the reference fluorophore of known quantum yield.

$$\Phi = \Phi_R \times \frac{I}{I_R} \times \frac{A_R}{A} \times \frac{\eta^2}{\eta_R^2}$$

Morphology Analyses

Field emission scanning electron microscopy (FESEM) techniques were used to examine their morphology. The morphology of PAM, PAD, PAD+Fe(III) complexes were photographed independently using a Carl Zeiss Gemini 300 FESEM. Before imaging, the samples were prepared by drop-casting 2 µL of desired solution combination on an Al-foil wrapped coverslip, then coating with Au and drying under vacuum.

Fluorescence Microscopy

The freshly prepared samples of PAD (5 µM) and PAD+Fe(III) (receptor 1 mixed with 10 equivalents of Fe(III)) glass slide, dried in air and images were taken after drying completely at room temperature followed by image acquisition using a fluorescence microscope (Olympus) using UV light.

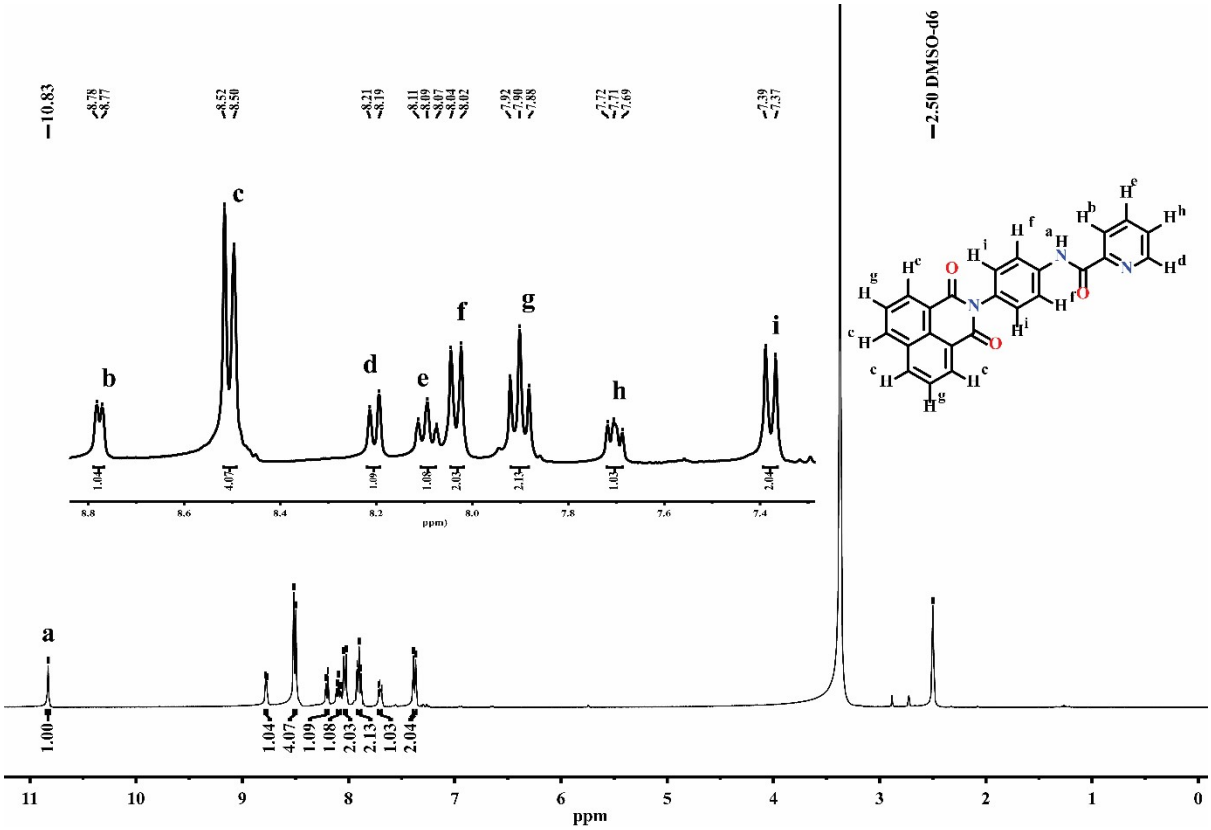

Fig. S1 ^{1}H NMR of PAM (DMSO-d_6, Room Temperature)

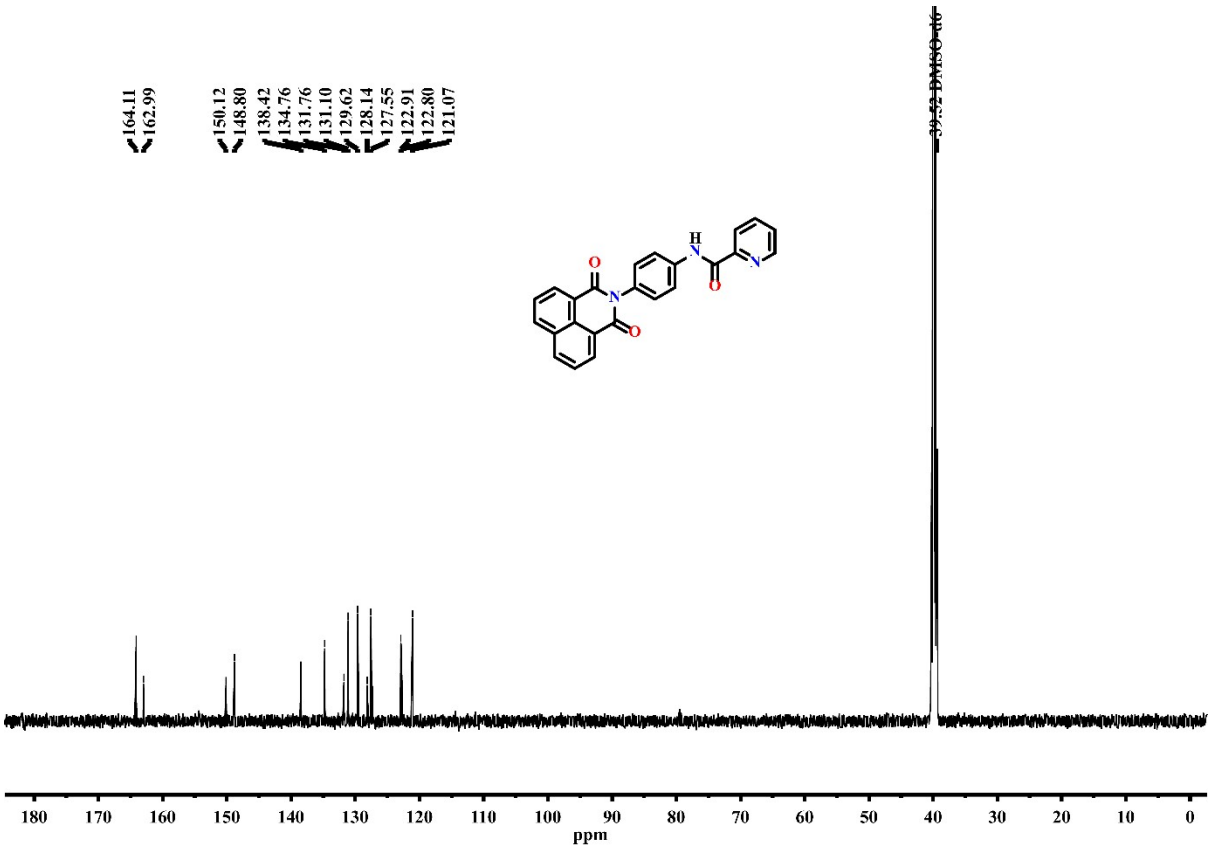

Fig. S2 ^{13}C NMR of PAM (DMSO-d_6, room temperature)

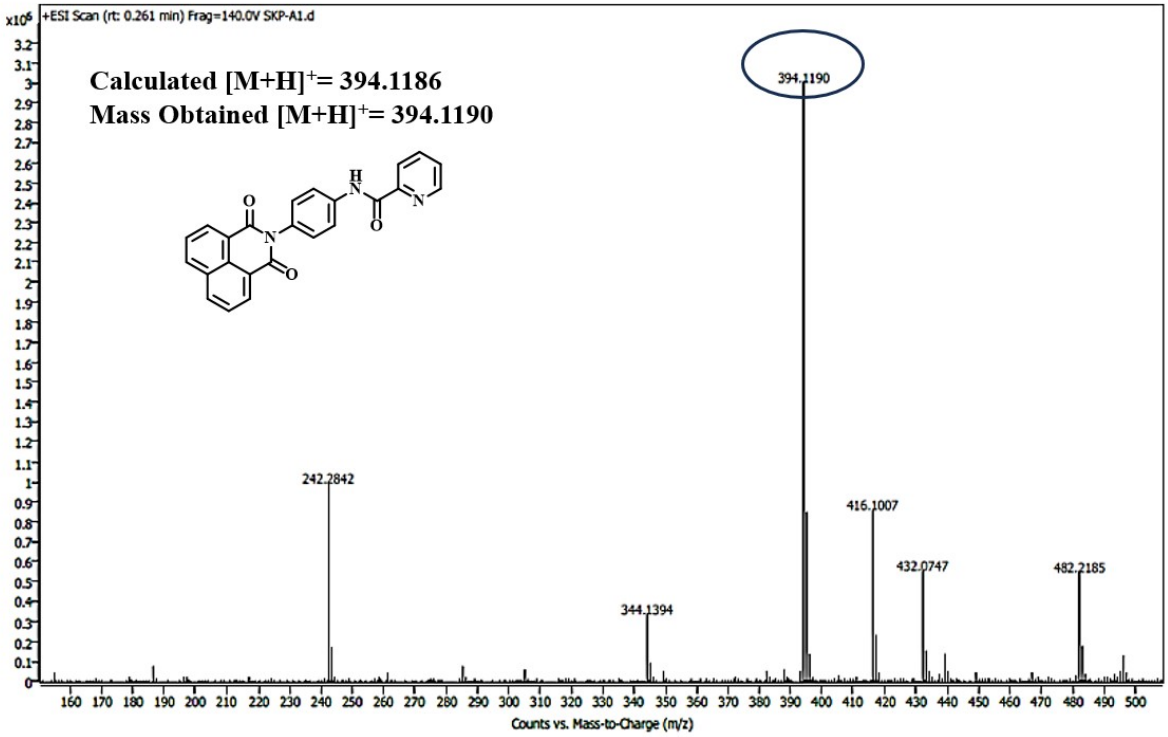

Fig. S3 HRMS of PAM.

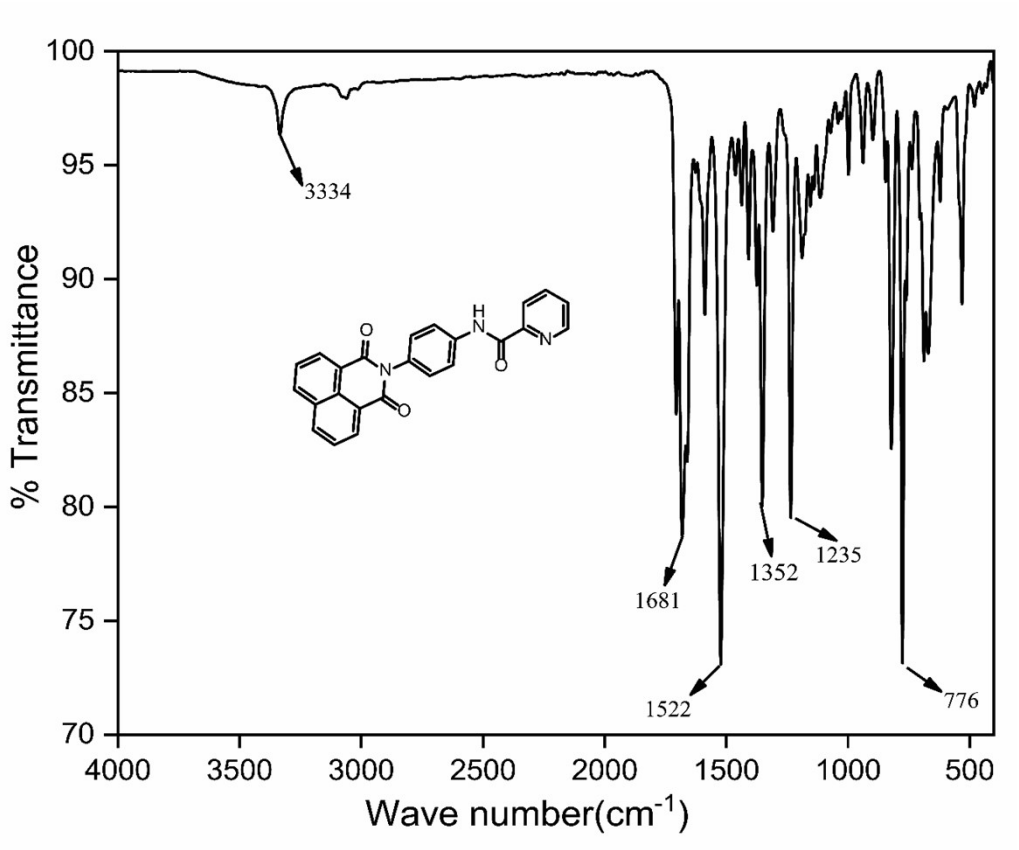

Fig. S4 FTIR Spectra of PAM.

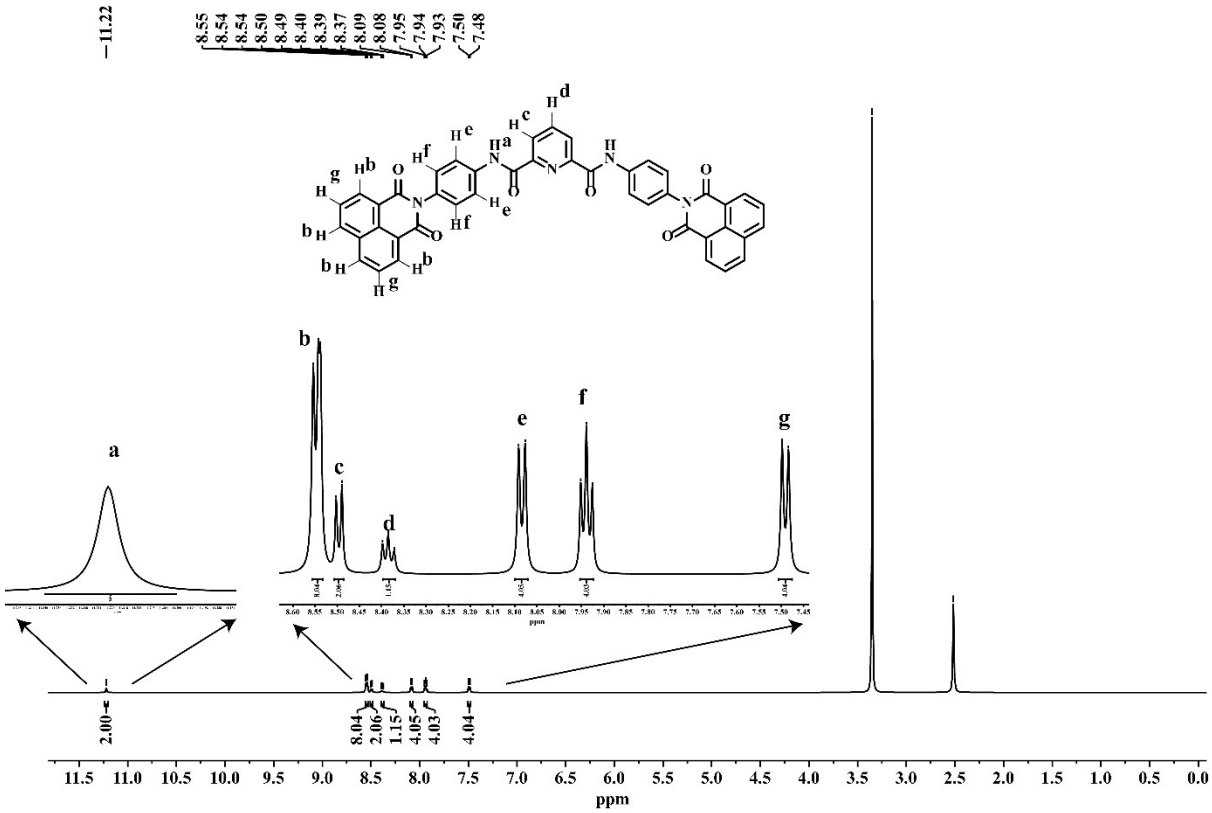

Fig. S5 ^{1}H NMR of PAD (DMSO-d_6, room temperature).

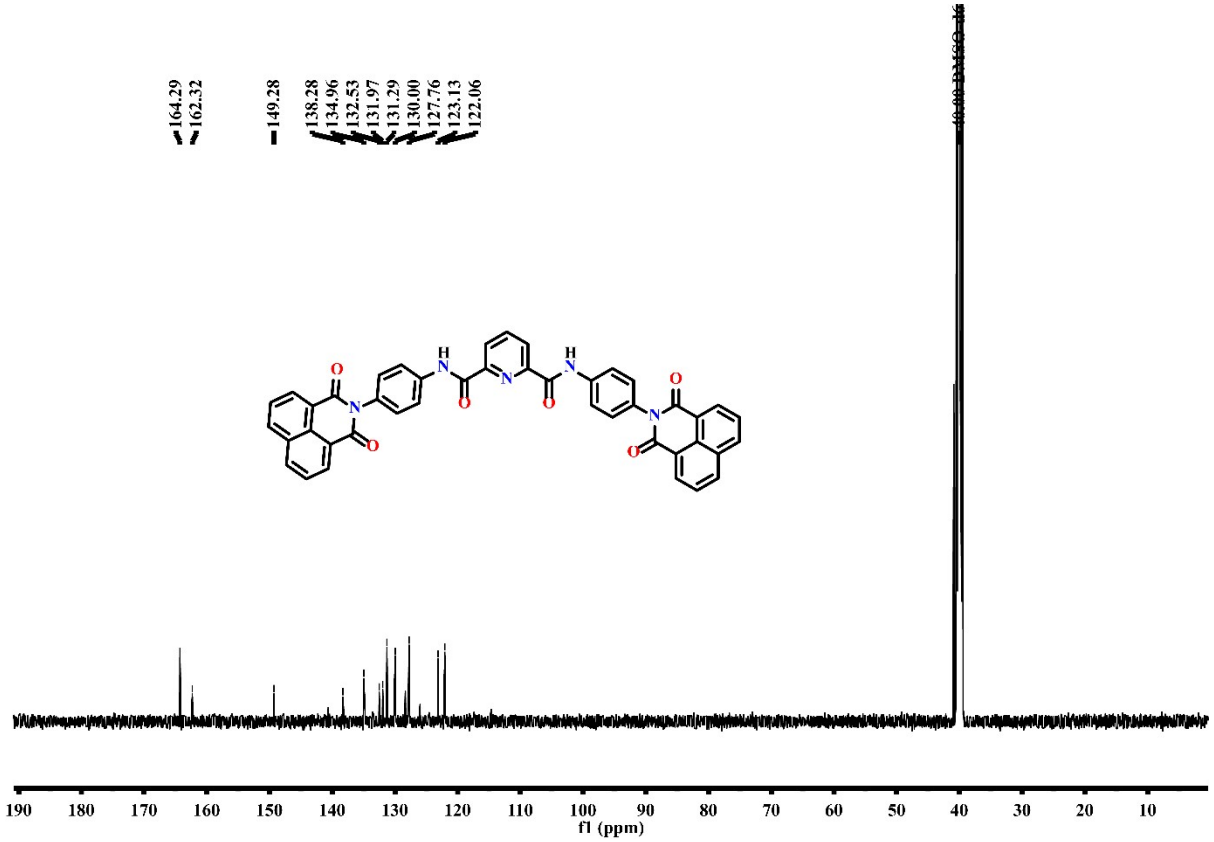

Fig. S6 ^{13}C NMR of PAD (DMSO-d_6, Room Temperature)

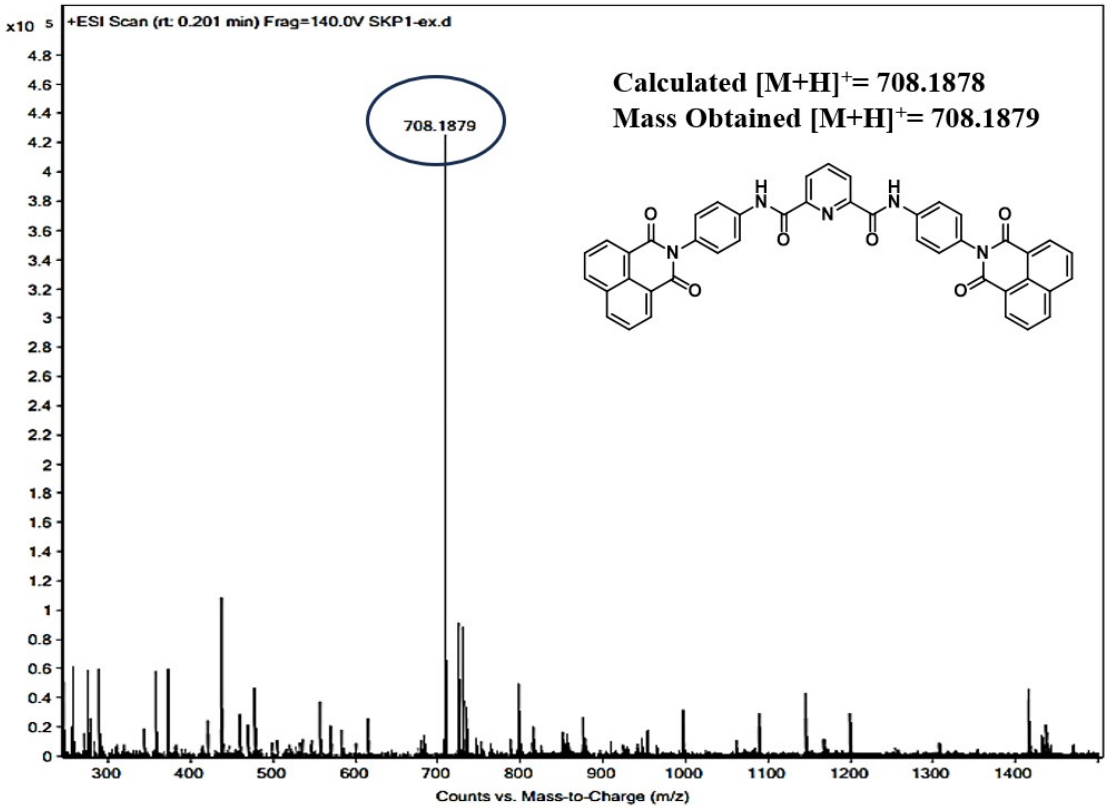

Fig. S7 HRMS of PAD

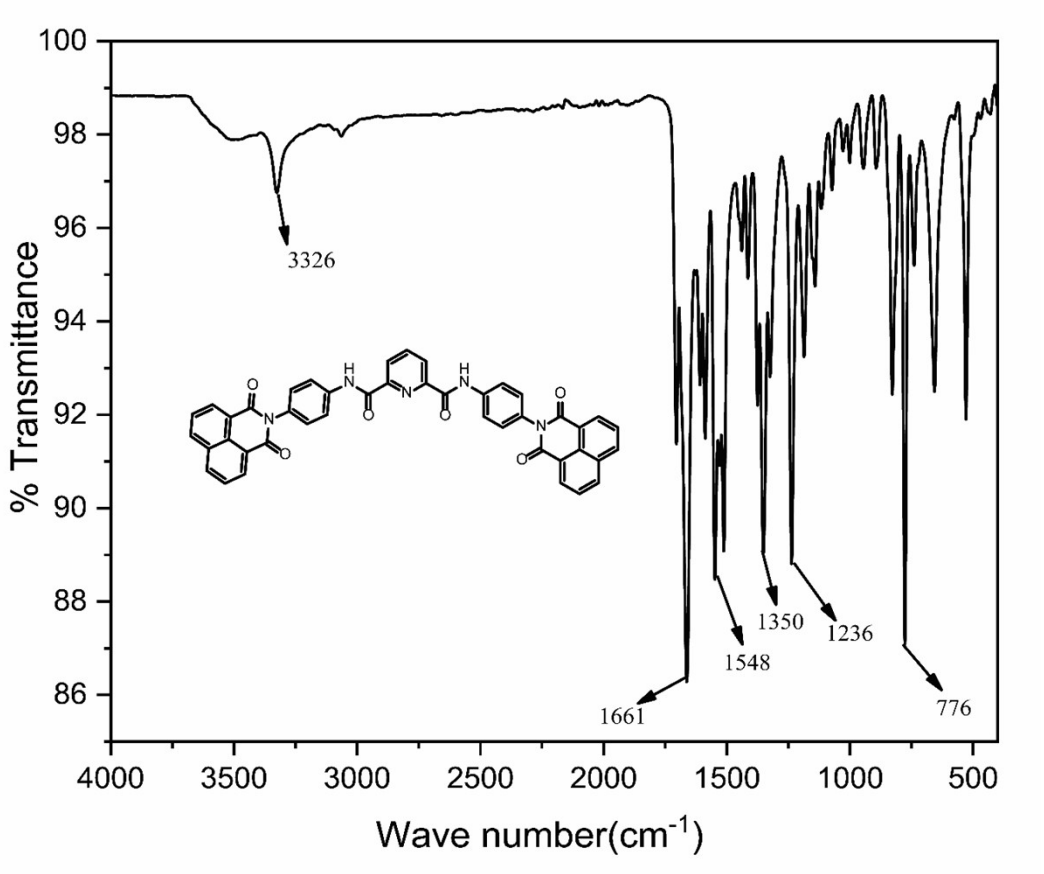

Fig. S8 FTIR spectra of PAD

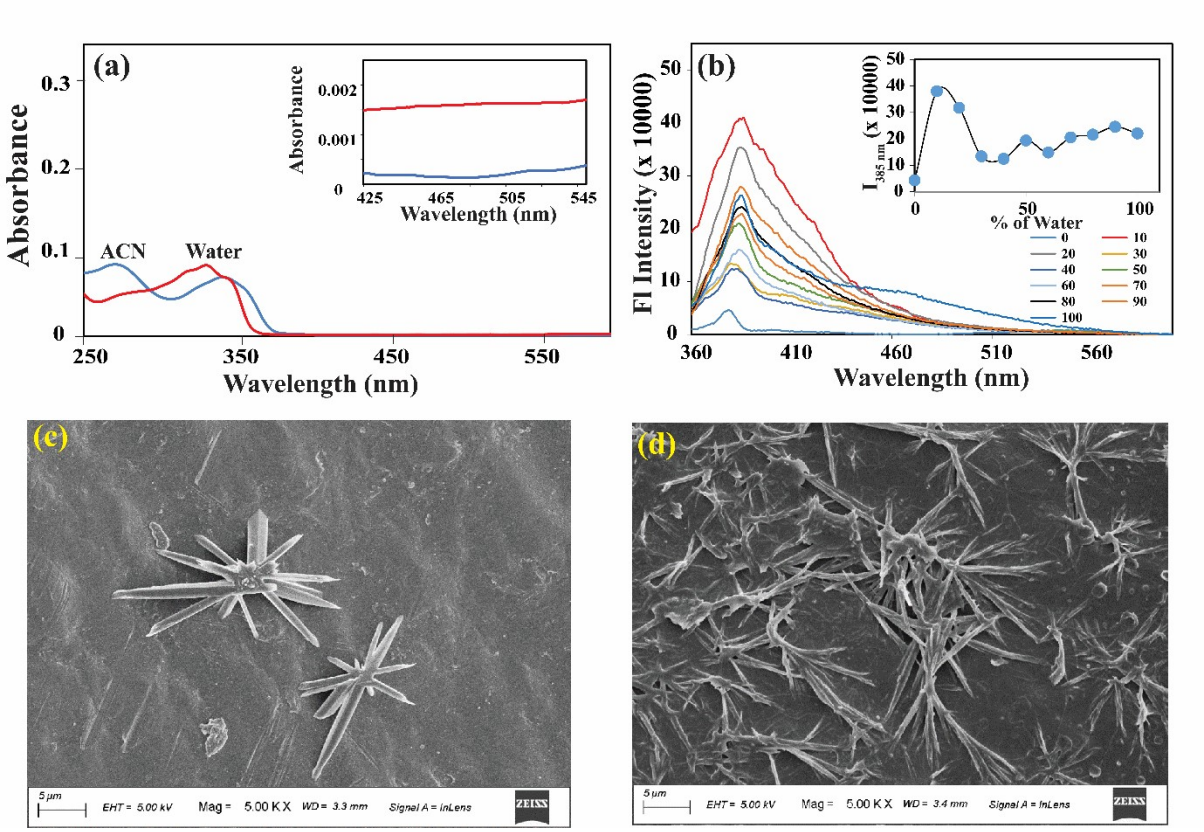

Fig. S9 (a) Absorption spectra in organic-blue line (ACN) and aqueous solvent-red line. (b) Emission spectroscopy plot with varying water percentage in ACN of PAM. FESEM Morphology of PAM in (c) Water (d) ACN

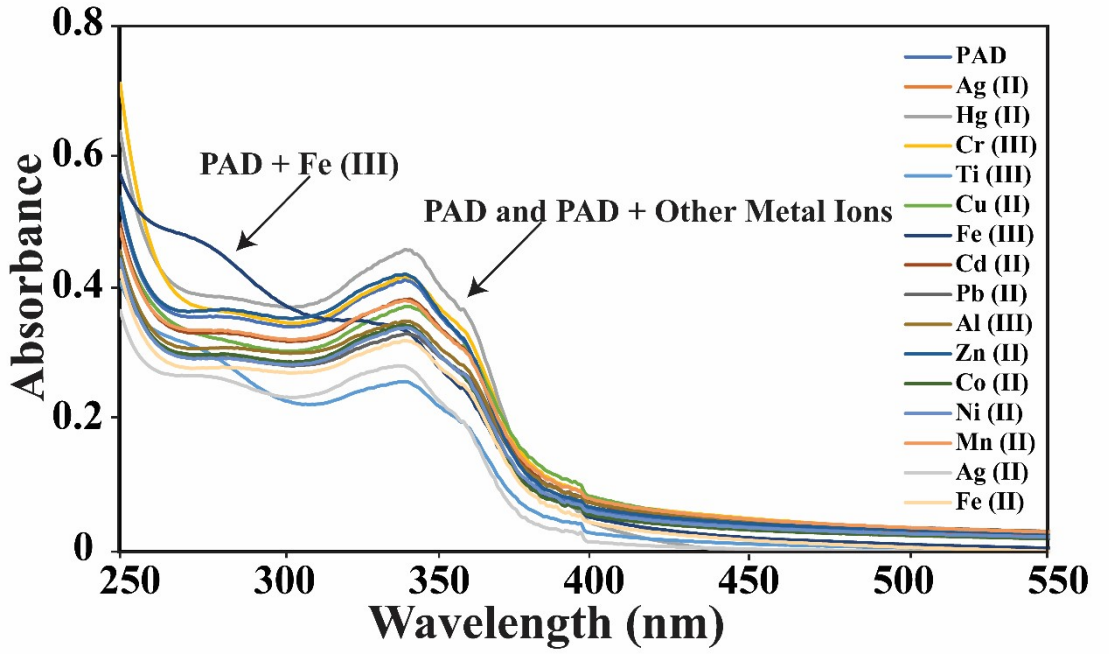

Fig. S10 Absorption spectra of PAD in presence of different cations

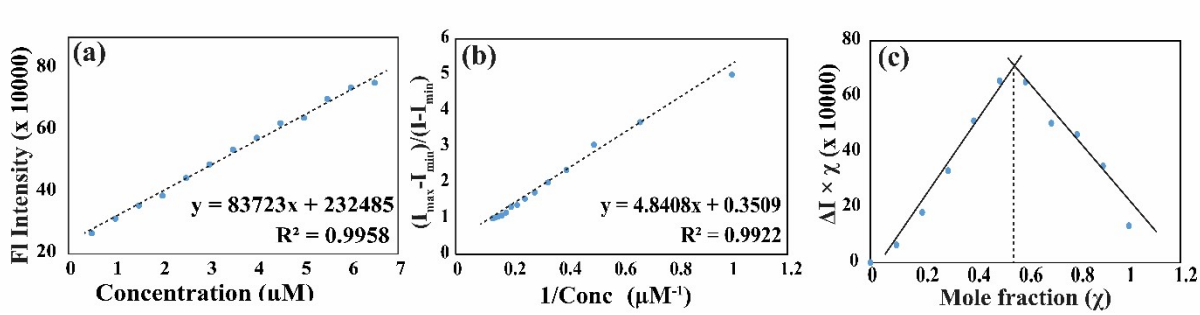

Fig. S11 (a) Linear relationship between the concentration of Fe(III) for the detection limit (LOD) calculation (b) B-H plot for determination of binding constant for Fe(III) (c) Job's plot showing 1:Fe(III) (1:1) complex.

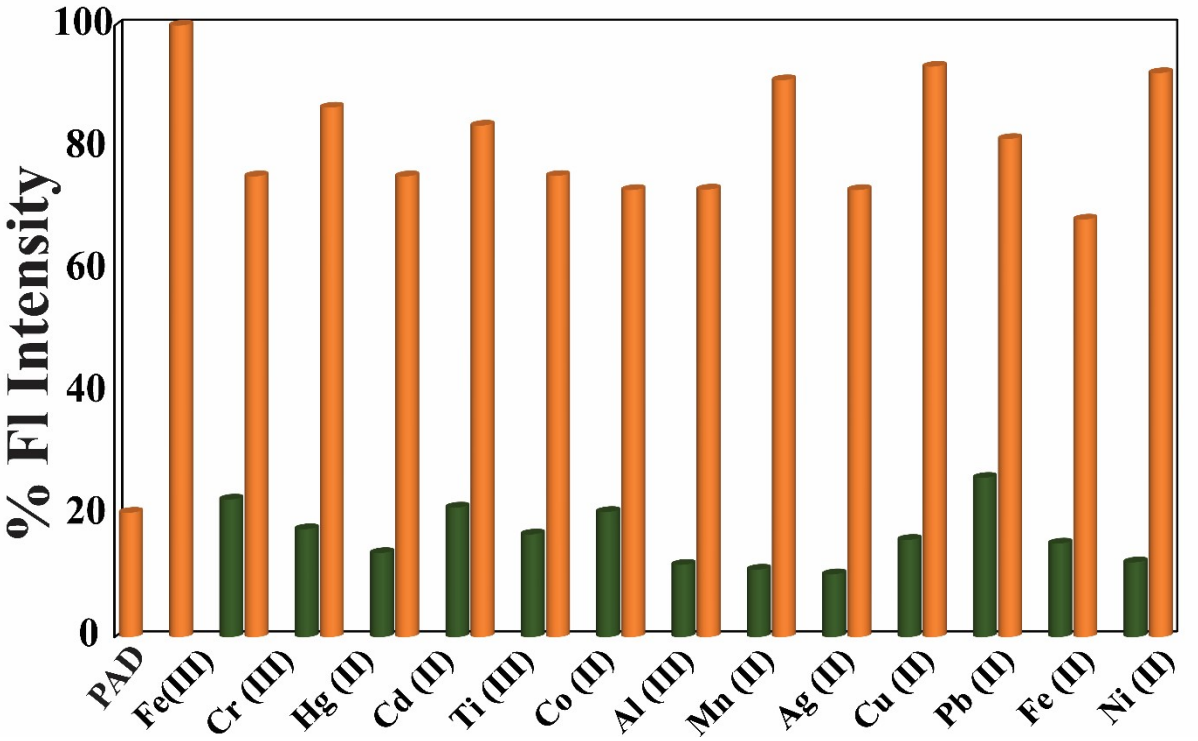

Fig. S12 Percentage Fluorescence response of PAD (5 μM); PAD and PAD+ Fe(III); PAD+Fe(III) + Other metal ions represented in orange color. PAD + Other metal ions represented in green color.

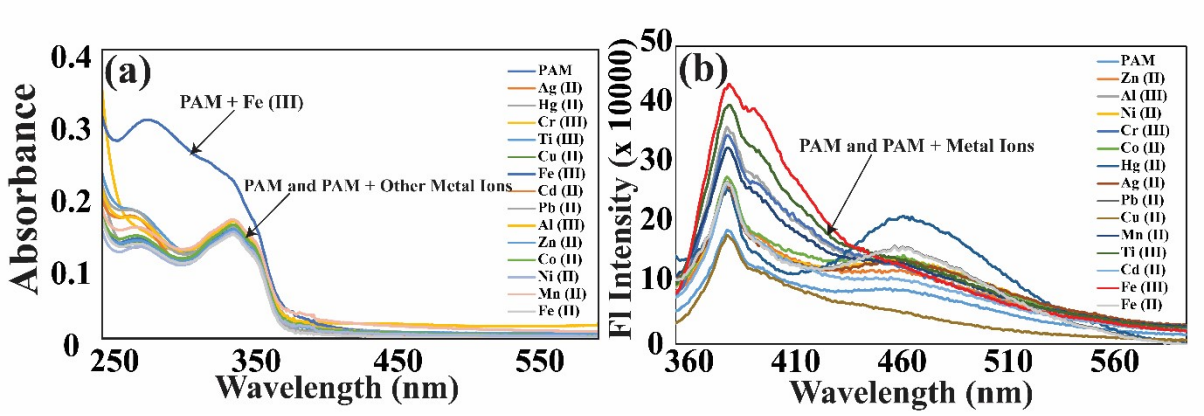

Fig. S13 (a) Absorption spectra of PAM in presence of different cations (b) Emission Spectra of PAM in presence of different cations (λ_{ex} 350 nm)

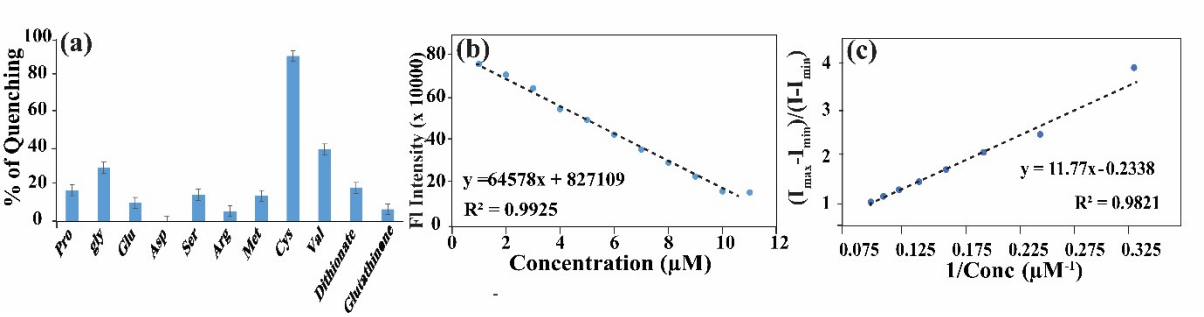

Fig. S14 (a) Bar Graph representing percentage of quenching in presence of different amino acids and bio-thiols (b) Linear relationship between the concentration of Fe (III) for the detection limit (LOD) calculation (c) B-H plot for determination of binding constant for Fe (III)

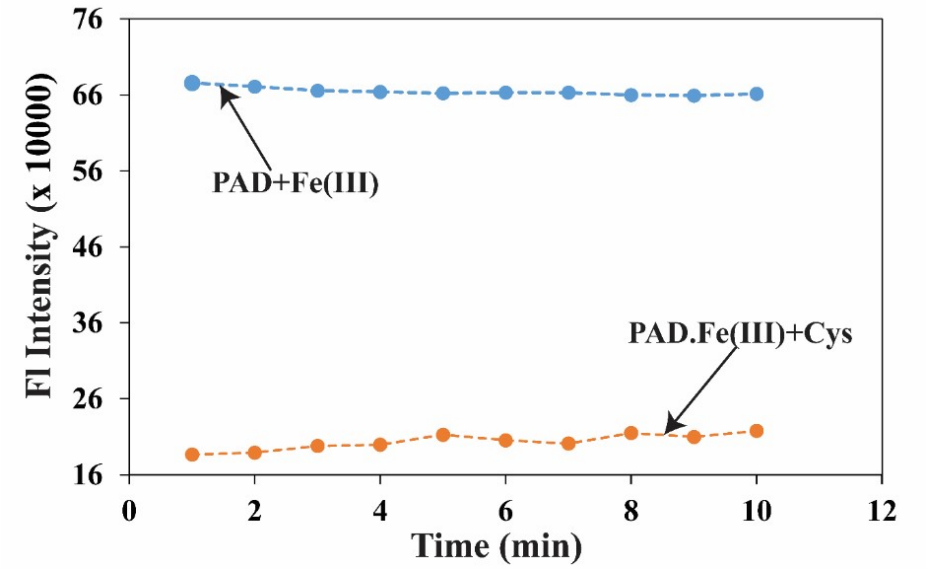

Fig. S15 Fluorescence response with respect to time on addition of Fe(III) – blue line; Addition of Cys to PAD⊂Fe(III) complex– orange line;

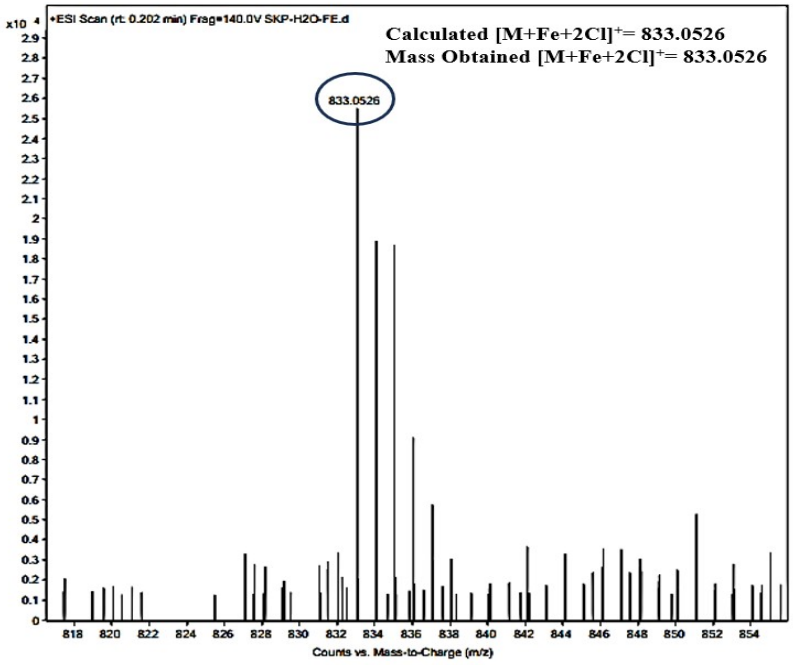

Fig. S16 ESI-MS spectra of PAD in water with Fe (III) in 1:1 ration in positive ionization mode

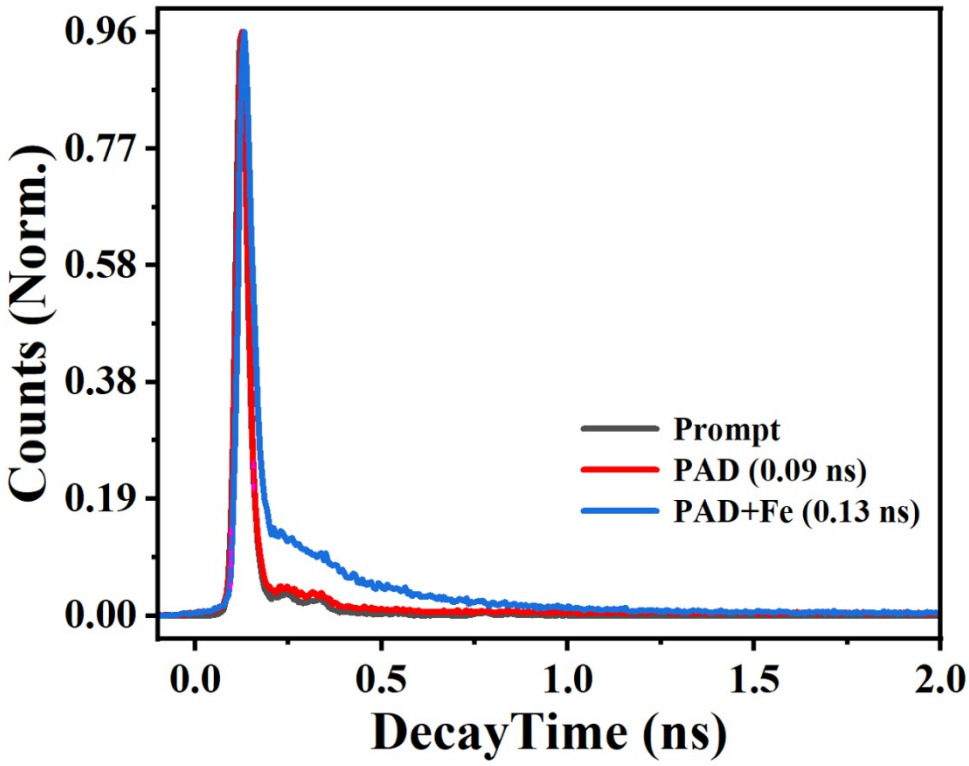

Fig. S17 Changes in Time-Resolved Photoluminescence (TRPL) decay of PAD and PAD+Fe in HEPES Buffer at Room temperature (Both having Single exponential decay)

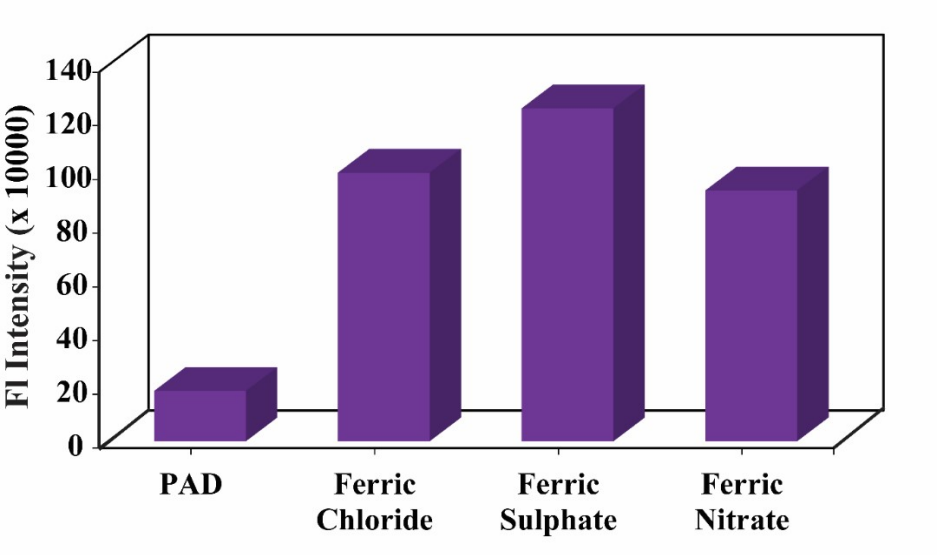

Fig. S18 Bar Graph representing percentage of enhancement in presence of different ferric salts

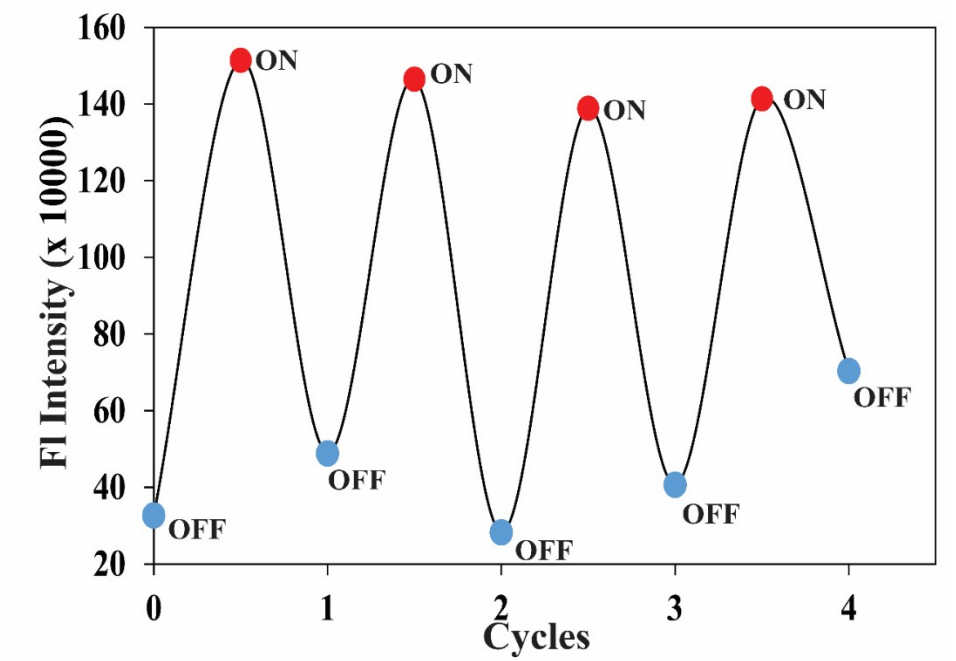

Fig. S19 Fluorescence intensity upon alternate addition of a constant amount of Fe(III) and Cysteine

Table S1 (Quantum Yield)

Sample	Integrated Emission	Abs at 350 nm	Refractive Index	Quantum Yield
Quinine Sulphate	2.41×E8	0.125	1.33	54%(Known)
PAD	2.27×E7	0.1225	1.33	4.3%
PAD+Fe(III)	9.40×E7	0.099	1.33	21.9%
PAD⊂Fe(III)+Cys	1.55×E7	0.0618	1.33	5.8%
PAM	1.15×E7	0.0578	1.33	4.6%

Crystallographic Refinement Details.

All the details of the refinement parameters of crystallographic data collection for the free receptors are furnished in **Table S1 and S2**, and also all of the above given data have been deposited into CCDC. A crystal of proper size was chosen for **PAM**, and the crystals were dipped into silicon oil prior to mounting into a glass fibre tube. Supernova (a single source at an offset) Eos diffractometer with Mo Kα radiation (λ = 0.71073 Å) source, connected with a CCD region detector was used to collect the X-ray intensity data and with the help of APEX 4 all the data refinement and cell reduction were done [16]. Using a narrow-frame algorithm and XPREP [17], the frames were combined with the Bruker SAINT software kit, and data were corrected for absorption effects using the multi-Scan process (SADABS) [18]. Using direct methods in XT, version 2014/15, all of the structures were solved and after that, refinement was done using the full-matrix least-squares technique in the SHELXL-2016 and 2018 software packages on F^2 [19]. The positions of the hydrogen atoms were fixed. We used MERCURY 4.2.0 for Windows for the sack of creating structural drawings [20]. The hydrogen atoms were found on a separate Fourier map and refined where it was most advantageous. For all non-hydrogen atoms Anisotropic refinement was employed.

Table S2. Crystallographic parameters and refinement data of the receptor PAM

Parameters	**PAM**
Formula	$C_{24}\ H_{15}\ N_3\ O_3$
Fw	393.39
cryst syst	monoclinic
space group	P 2/c
a (Å)	6.774 (2)
b (Å)	13.257 (4)
c (Å)	20.637 (6)
α (deg)	90
β (deg)	97.183(8)
γ (deg)	90
V ($Å^3$)	1838.8(9)
Z	4
DC ($g\ cm^{-3}$)	1.421
μ (Mo Kα) (mm^{-1})	0.096
F (000)	816.0
T (K)	300 K
θmax (deg)	24.998
total no. of rflns	22767
no. of indep rflns	3221
no. of obsd rflns	1552
no.of params refined	272
R1, $I > 2\sigma(I)$	0.1464(1552)
wR2, $I > 2\sigma(I)$	0.4682(3221)
GOF (F^2)	1.510
CCDC no.	2305044

Table S3. Crystallographic parameters and refinement data of the receptors PAM

D H···A	d(D···H)/Å	d(H···A)/Å	d(D···A)/Å	<D-H···A/	Symmetry codes
N2-H5···N1	0.86	2.16	2.605 (10)	112	x, y, z
C2-H2···O2	0.93	2.39	3.231 (14)	150	x, -y, -1/2+z,
C3-H3···O2	0.93	2.60	3.514 (17)	168	-x, -y, -z
C9-H7···O1	0.93	2.36	2.912 (11)	118	x, y, z

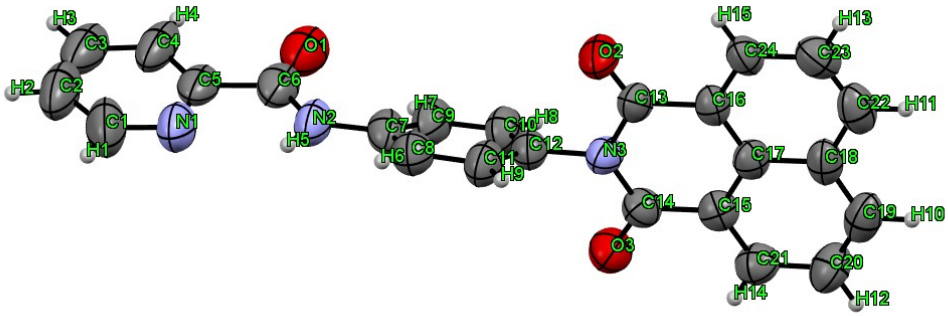

Fig. S20 SC-XRD view of receptor in 50% ellipsoid occupancy.

Table S4 Comparison of some reported ferric ion receptor with the present work.

Receptor	**Fluorescence Behaviour**	**Solent System**	**Limit of Detection**	**Reference**
Naphthalimide-based catechol moiety	Quenching	10 mM MES aqueous buffer of pH 4.5.	0.44 μM	2
Triazole and pyridine moieties (TPE–TAP)	Quenching	THF–H2O (2 :98 v/v%)	1.3 μM	3
Triphenylamine (TPA) based	Quenching	water: THF; 4:1, v/v	19 nM	4
Carbazole-based	Quenching	DMSO	1.38 nM	5
Anthracene based	Quenching	DMSO-H2O	5.09 μM	6
Triphenylamine based (TTU)	Quenching	H2O/THF (6:4, v/v)	0.14 ppm	7
AZO based	Enhancement	acetonitrile	1.3 nM	8
Boron dipyrromethene (BODIPY)	Quenching	DMF	3.75 μM	9
Coumarin Derived	Enhancement	DMSO/H2O (1:9, v/v, pH = 7.2)	0.48 μM	10
Naphthalenecarboxamide	Quenching	DMSO-H2O (8:2 v/v)	0.51 μM	11
Pyridine Derived	Enhancement	HEPES Buffer (1 mM)	0.81 μM	(THIS WORK)

Table S5. Comparison of some reported metal based receptor for Cysteine with the present work

Receptor	**Fluorescence Behaviour Restoration**	**Solent System**	**Limit of Detection**	**Reference**
TBT-Hg (II)	100%	water/DMF (1:1, v/v)	104.1 nM	12
Lc-NBD-Cu (II)		HEPES-SDS buffer (10 mM, pH = 7.4)	0.78 μM.	13
Pyr-1-Fe (III)		1% DMSO)	0.44 μM.	14
PCZBTA-TBZ-Cu (II)	67%	THF		15
PAD-Fe (III)	Enhancement	HEPES Buffer (0.1 mM)	0.81 μM	(THIS WORK)

References

S1. Q. Lin, X. W. Guan, Y. Q. Fan, J. Wang, L. Liu, J. Liu, H. Yao, Y. M. Zhang, *New J. Chem.,* 2019, **43**, 2030-2036

S2. A. Silswal, P. Weslie and A.L. Koner, *Talanta*, 2023, **254**, 124147.

S3. O. Dalkilic, E. Bozkurt, F. Lafzi and H. Kilic, *Org. Biomol. Chem.*, 2023, **21**, 5406-5412.

S4. M.A. Assiri, S. Hanif, H.M. Junaid, A. Hamad, H. Irshad, M. Yar, W. Rauf and S.A. Shahzad, *J. Photochem. Photo. A*, 2023, **438**, 114514.

S5. A. Battal, S.B. Kassa, N.A. Gultekin, M. Tavasli and Y. Onganer, *J. Fluoresc.*, 2023, **33**, 1-9.

S6. T. Verma, P. Verma and U.P. Singh, *Microchem. J.*, 2023, **191**, 108771.

S7. A.Y.A. Alzahrani, K.O. Khan, S. Rafique, H. Irshad, A.M. Khan and S.A. Shahzad, *Spectrochim. Acta A Mol. Biomol. Spectrosc.*, 2023, **297**, 122745.

S8. M. Saremi, A. Kakanejadifard, M. Ghasemian and M. Namdari, *J. Mol. Struct,*, 2023, **1283**, 135289.

S9. C. Li, Q. Sun, Q. Zhao and X. Cheng, *Spectrochim. Acta A Mol. Biomol. Spectrosc.*, 2020, **228**, 117720.

S10. Z.Y. Yin, J.H. Hu, K. Gui, Q.Q. Fu, Y. Yao, F.L. Zhou, L.L. Ma and Z.P. Zhang, *J. Photochem. Photo., A*, 2020, **396**, 112542

S11. B. Tavakoli, S. Meghdadi, Z. Salarvand, K. Eskandari, A. Amiri and M. Amirnasr, *J. Photochem. Photo., A*, 2023, **440**, 114661.

S12. H. Irshad, M.A. Assiri, S. Rafique, A.M. Khan, M. Imran and S.A. Shahzad, *Spectrochim. Acta A Mol. Biomol. Spectrosc.*, 2023, **300**, 122934.

S13. W. Wang, L. Jiang, W. Wang, Y. Chen, J. Peng, Y. Wang, Y. Jiao, Y. Li, X. Jiang, S. Lu, and F. Wang, *Spectrochim. Acta A Mol. Biomol. Spectrosc.*, 2023, **301**, 122942.

S14. Y. Hu, L. Lu, S. Guo, X. Wu, J. Zhang, C. Zhou, H. Fu and Y. She, *Sens. Actuators B Chem.*, 2023, **382**, 133534.

S15. L. Gao, J. Xu, H. Luo, H. Lei, X. Chen, J. Wan, J. Feng and K. Liu, *J. Fluoresc.*, 2023, **33**, 1-15.

S16. Apex 4; Bruker AXS Inc.: 2016.

S17. *SMART, SAINT, and XPREP*, Siemens Analytical X-ray Instruments Inc., Madison, WI, 1995.

S18. G. M. Sheldrick, SADABS, *Program for Area Detector Adsorption Correction*; Institute for Inorganic Chemistry, University of Göttingen, 1996.

S19. G. M. Sheldrick, *Acta Crystallogr., Sect. C: Struct. Chem.*, 2015, **71**, 3.

S20. C. F. Macrae, I. Sovago, S. J. Cottrell, P. T. A. Galek, P. McCabe, E. Pidcock, M. Platings, G. P. Shields, J. S. Stevens, M. Towler, P. A. Wood, *J. Appl. Crystallogr.*, 2020, **53**, 226.